VIP Li–O_2 Batteries Very Important Paper

Deutsche Ausgabe: DOI: 10.1002/ange.201907477
Internationale Ausgabe: DOI: 10.1002/anie.201907477

Vanadium(III) Acetylacetonate as an Efficient Soluble Catalyst for Lithium–Oxygen Batteries

*Qin Zhao, Naman Katyal, Ieuan D. Seymour, Graeme Henkelman, and Tianyi Ma**

Abstract: *High donor number (DN) solvents in Li—O_2 batteries that dissolve superoxide intermediates in lithium peroxide (Li_2O_2) formation facilitate high capacities at high rates and avoid early cell death. However, their beneficial characteristics also result in an instability towards highly reactive superoxide intermediates. Furthermore, Li—O_2 batteries would deliver a superior energy density, but the multiphase electrochemical reactions are difficult to achieve when operating with only solid catalysts. Herein we demonstrate that vanadium(III) acetylacetonate ($V(acac)_3$) is an efficient soluble catalyst that can address these problems. During discharge, $V(acac)_3$ integrates with the superoxide intermediate, accelerating O_2 reduction kinetics and reducing side reactions. During charge, $V(acac)_3$ acts as a redox mediator that permits efficient oxidation of Li_2O_2. The cells with $V(acac)_3$ exhibit low overpotential, high rate performance, and considerable cycle stability.*

With the ever-growing demand for electric vehicles, the requirements for next-generation batteries with high energy density have increased.[1] The theoretical energy density of Li–O_2 batteries is extremely high (ca. 3500 $Wh\,kg^{-1}$) so that the system has attracted much attention.[2] However, Li–O_2 batteries also have severe problems that must be addressed before they can be used in practical applications. The key issues for Li–O_2 batteries are the high charge voltage, severe side reactions, and low cycle life.[3] Although these drawbacks are interrelated to some extent, the low cycle life is often ascribed to the insulating properties of the discharge product (Li_2O_2) and side reactions in Li–O_2 batteries.[4] The low conductivity of Li_2O_2 weakens the oxygen evolution reaction (OER) and raises the charge voltage, which causes the side reactions. Equally important, the formation of Li_2O_2 is irregularly distributed on the O_2 electrode, which can block the porous O_2 electrode and hinder the efficient transport of electrons and ions. Therefore, promoting the efficient decomposition of Li_2O_2 to reduce the charge voltage is the key to improving the cycle life of Li–O_2 batteries.[5] In early studies, researchers introduced OER or water-splitting catalysts into Li–O_2 batteries to overcome these drawbacks.[6] Though these catalysts exhibited good performance in Li–O_2 batteries,[7] it has also been reported that some catalysts promote the decomposition of the electrolyte while facilitating the oxidation of Li_2O_2.[8] Moreover, these catalysts are generally in the solid state in which the active sites are limited to the interface with Li_2O_2, which results in low utilization of the catalysts. It has been reported that the use of soluble catalysts can accelerate the Li_2O_2 decomposition, reduce charge voltage, and improve the cyclability in Li–O_2 batteries.[9]

The soluble catalyst reversibly accepts and donates electrons at a higher potential than the equilibrium potential of Li_2O_2 formation/decomposition, which facilitates the oxygen evolution reaction (OER) at the interface of electrolyte–Li_2O_2. Upon charging, a soluble catalyst is oxidized at the surface of the electrode, diffuses to the surface of Li_2O_2 through the electrolyte, and is then reversibly reduced by Li_2O_2, which is oxidized to evolve O_2.[10] Several types of soluble catalysts have been reported, such as tetrathiafulvalene (TTF),[9a] lithium iodide (LiI),[11] lithium bromide (LiBr),[9b,12] tetramethyl Piperidinyloxy (TEMPO),[13] iron phthalocyanine (FePc),[14] and 5,10-dimethylphenazine (DMPZ).[10a] These soluble catalysts significantly lower the charge voltage and reduce side reactions.[15] High DN solvents are especially good at promoting high capacities at high rates by facilitating lithium superoxide intermediate dissolution and reversibility of Li–O_2 batteries. Nevertheless, proton abstraction or nucleophilic attack by the highly reactive O_2 reduction intermediate leads to undesirable side reactions during discharge, especially in high DN solvents with high polarity.[2b] However, the development of a soluble bifunctional catalyst that is able to reduce both side reactions, which arise from superoxide intermediates during discharge, as well as permit efficient oxidation of solid Li_2O_2, remains a formidable challenge.

Herein we demonstrate the use of a bifunctional $V(acac)_3$ soluble catalyst in a Li–O_2 battery, which tunes the ORR mechanism by controlling superoxide intermediates and reduces the charge voltage by transporting electrons in the electrolyte. We show that this catalyst thereby efficiently reduces side reactions and enhances the cyclability of a Li–O_2 battery.

Figure 1 a shows cyclic voltammetric (CV) curves of 5 mM $V(acac)_3$ in a solution of dry dimethyl sulfoxide (DMSO)

[*] Dr. Q. Zhao
Institute of Clean Energy Chemistry, Key Laboratory for Green Synthesis and Preparative Chemistry of Advanced Materials, College of Chemistry, Liaoning University
Shenyang 110036 (China)
N. Katyal, Dr. I. D. Seymour, Prof. G. Henkelman
Department of Chemistry, The Oden Institute for Computational Engineering and Sciences, The University of Texas at Austin
105 E. 24th Street, Stop A5300, Austin, Texas 78712 (USA)
Dr. Q. Zhao, Dr. T.-Y. Ma
Discipline of Chemistry
The University of Newcastle
Callaghan, NSW 2308 (Australia)
E-mail: Tianyi.Ma@newcastle.edu.au
Supporting information and the ORCID identification number(s) for the author(s) of this article can be found under: https://doi.org/10.1002/anie.201907477.

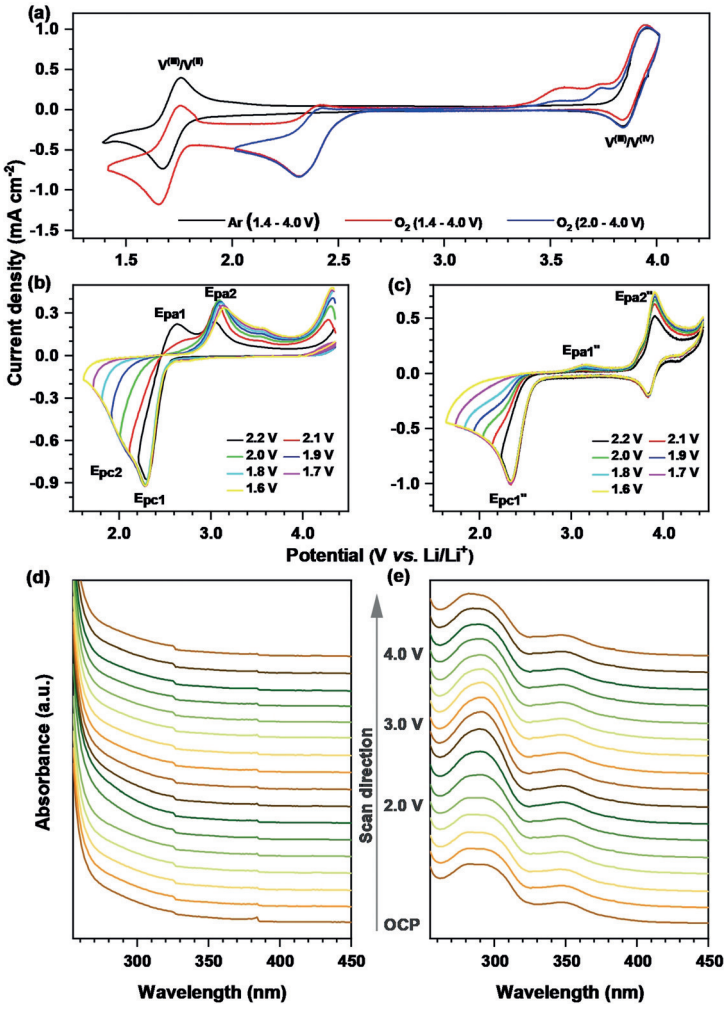

Figure 1. a) Cyclic voltammetry of $V(acac)_3$ on a glassy carbon electrode under an Ar and O_2 atmosphere at a scan rate of 100 $mV s^{-1}$ with a potential range of 1.4–4.0 V or 2.0–4.0 V in TBA^+-containing electrolyte. Cyclic voltammetry of the Li^+-containing electrolyte b) without $V(acac)_3$ and c) with $V(acac)_3$ at a scan rate of 100 $mV s^{-1}$ with varying potential ranges. In situ UV/Vis spectra of the electrolyte d) without $V(acac)_3$ and e) with $V(acac)_3$ at a scan rate of 10 $mV s^{-1}$ with the scan direction of the open circuit potential (OCP) → 2.0 V → 4.0 V.

containing 0.1 M tetrabutylammonium perchlorate ($TBAClO_4$) as the supporting salt on a glassy carbon electrode under an Ar and O_2 atmosphere at a scan rate of 100 $mV s^{-1}$. In the absence of O_2, the $V(acac)_3$ CV reveals two pairs of well-defined redox couples between 1.40–4.00 V, which can be attributed to V^{III}/V^{II} and V^{III}/V^{IV}.[16] The redox couple of V^{III}/V^{IV} at 3.90 V exceeds the equilibrium potential of Li_2O_2 formation/decomposition, which is compatible with oxidizing solid Li_2O_2. In the presence of O_2, CVs with two different potential ranges are performed to verify the effect of the V^{III}/V^{II} redox couple on ORR. In the potential range of 2.00–4.00 V, the scan is reversed at the half-peak potential (2.43 V) of the cathodic peak corresponding to the ORR. When the potential range is enlarged to 1.40–4.00 V, the O_2 reduction peak overlaps with that of the potential range of 2.00–4.00 V, no other reduction peak can be observed, which demonstrates that the V^{III}/V^{II} couple might not be involved in ORR. The return anodic scan indicates continuous oxidation of the O_2 reduction product when the potential is above 3.30 V, signifying that multiple steps are involved and a more complex electrode reaction than has been reported.[17] The superoxide intermediate is a relatively soft Lewis base that forms stable complexes in the electrolyte containing soft Lewis acid (TBA^+) in accordance with Pearson's hard soft acid base (HSAB) theory, which prevents it from reducing further.[18] Therefore, the O_2 reduction involves the formation of superoxide with a reversible one-electron couple in an electrolyte without $V(acac)_3$ (Figures S1 a, b in the Supporting Information). However, two-electron reduction is the dominant reaction for the electrolyte with $V(acac)_3$ (Figures S1 c, d), which indicates that $V(acac)_3$ changes the ORR mechanism in TBA^+-containing electrolyte. Different from TBA^+, Li^+ is a hard Lewis acid, which has a high affinity for a hard Lewis base (peroxide) according to the HSAB theory. However, the acidity of Li^+ can be reduced in high DN solvents, which facilitates the superoxide intermediate. To understand the effect of soluble catalysts on the ORR process in the Li^+-containing electrolyte, CVs with and without $V(acac)_3$ are carried out within specific electrochemical windows.

For the ORR without $V(acac)_3$ (Figure 1 b), the scan is reversed at the half-peak potential (2.42 V) of the first cathodic peak (E_{pc1}) in the potential range of 2.20–4.40 V. Reversing the scan results in two clear anodic peaks at 2.63 V (E_{pa1}, superoxide) and 3.05 V (E_{pa2}, peroxide), indicating a dual step reduction mechanism. From the in situ UV/Vis absorption spectra in Figure 1 d, increased absorbance in the wavelength range of 260–280 nm can be observed after the ORR begins, verifying that a superoxide intermediate is generated. Upon further scanning cathodically (2.00–4.40 V), the current slope varies at 2.10 V, indicating another electrochemical process (E_{pc2}). A subsequent reverse scan in the positive direction results in a decrease of E_{pa1} and an increase of E_{pa2}, suggesting the consumption and conversion of the first reduction product into the second reduction product, which is oxidized at E_{pa2}.[19] The high DN of the DMSO solvent (29.8) lowers the Lewis acidity of the solvated Li^+ and makes the superoxide ion pair complex more stable by suppressing its tendency to disproportionate. This effect promotes the solubility of lithium superoxide (LiO_2) and increases the capacity of the Li–O_2 battery. Nevertheless, highly reactive superoxide intermediates could attack the high DN solvent and the positive active materials, causing side reactions that are adverse to the long-term cycling stability.[20]

For the ORR with $V(acac)_3$, the scan is reversed at the half-peak potential (2.49 V) of the first cathodic peak (E_{pc1}'') in the potential range of 2.2–4.4 V (Figure 1 c). Reversing the scan results in two clear anodic peaks at 3.12 V (E_{pa1}'') and 3.91 V (E_{pa2}''). The E_{pa1}'' peak can be attributed to the oxidation of amorphous Li_2O_2.[21] The E_{pa2}'' peak corresponds to the electrochemical oxidation of the $V(acac)_3$, which in turn chemically oxidizes the solid Li_2O_2. No peak correspond-

ing to the oxidation of superoxide is observed. Upon further scanning cathodically, no other reduction peaks are detected. Reverse scanning anodically results in the increase in the E_{pa1}'' and E_{pa2}'' peak current densities. To better elucidate chemical changes of the $V(acac)_3$ at different electrochemical states, in situ UV/Vis absorption spectra were conducted (Figure 1e). The absorption of peaks at 279 and 292 nm are assigned to the π–π* band caused by the interaction between the metal and the ligand. The shoulder peak at 343 nm can be assigned to the electron transfer band (d_ε–π*).[22] In the cathodic scan, the absorbance at 292 nm clearly increases, which can be attributed to the strong absorption of $V(acac)_3$ to the superoxide intermediate in the electrolyte. This interaction can be proved by adding potassium superoxide (KO_2) in the soluble catalyst containing electrolyte (Figure S2). In the reverse scan, the absorbance at 292 nm gradually reduces, indicating the recovery of $V(acac)_3$, which highlights the reversibility of the redox process. Hence, the $V(acac)_3$ soluble catalyst integrates with the superoxide species during ORR and promotes the electron transport in solution during OER, which reduces the side reactions during discharge and charge in the Li–O_2 battery.

Figures 2a,b depict the discharge–charge curves of Li–O_2 cells without and with $V(acac)_3$ at different current densities with a capacity limit of 500 mAh g^{-1}. Compared with the cells without the $V(acac)_3$ soluble catalyst, the Li–O_2 cells with $V(acac)_3$ exhibit lower discharge and charge overpotentials and higher coulombic efficiency at corresponding current densities. At the high current density of 1000 mA g^{-1}, the discharge voltage plateau of the cell with $V(acac)_3$ is slightly reduced to 2.7 V, and a specific charge capacity of 435 mAh g^{-1} is delivered at a low charge plateau (3.90 V). In contrast, the discharge voltage plateau of the cell without $V(acac)_3$ is sharply reduced to 2.30 V, and the charge voltage is increased to 4.20 V, and only 191 mAh g^{-1} specific charge capacity is delivered. These results indicate that the $V(acac)_3$ soluble catalyst not only facilitates a high rate performance by the interaction with the superoxide intermediate but also promotes Li_2O_2 decomposition at a lower charge voltage. In addition, as shown in Figures 2c,d, the cell with $V(acac)_3$ exhibits an enhanced cycle life (100 cycles) compared with that of the cell without $V(acac)_3$ (14 cycles; Figure S3). The termination voltage of the cell with $V(acac)_3$ remains stable, which further indicates good cycle stability.

The reversibility of the cell with the $V(acac)_3$ soluble catalyst is further supported by the XRD and SEM measurements. The diffraction peaks of the discharged electrode, centered at 32.7°, 34.9°, and 58.6°, are assigned to Li_2O_2 after discharge (Figure 3a). X-ray photoelectron spectra (XPS) of the O_2 electrode indicate Li_2O_2 as the main discharge product; no other by-products were detected (Figure S4). Interestingly, the soluble catalyst changes the morphology of Li_2O_2 on the electrode into toroid-like and film-like products coexisting after discharge (Figure 3b), which is quite different from the cell without $V(acac)_3$ (Figure S5).[5c] The difference in morphology of the discharge product could be due to the unique discharge process catalyzed by $V(acac)_3$. After a subsequent charge progress, all of the XRD diffraction peaks attributed to Li_2O_2 disappear and the morphology of the O_2 electrode is recovered, indicating superior reversibility of the cell with $V(acac)_3$. In addition, UV/Vis spectroscopic titration and modified iodometric titration methods are performed to quantify the reversibility of the cells without or with the $V(acac)_3$ soluble catalyst. Figures 3c,d demonstrate the capacity values determined by the UV/Vis spectroscopic titration of Li_2O_2 in the discharged and charged electrodes. The O_2 electrode discharged to a capacity of 1 mAh can be titrated to obtain about 0.88 mAh in the absence of $V(acac)_3$. Two possible pathways can explain the low capacity retention. On the one hand, some part of Li_2O_2 (or LiO_2) is consumed by side reactions with the carbonaceous electrode and/or electrolyte producing by-products. On the other, the hydrolysis of LiO_2 that exists in the discharge products in the high DN solvent does not produce H_2O_2, resulting in a low titration value.[23] For the O_2 electrode cycled in the presence of $V(acac)_3$, a capacity of 0.92 mAh can be titrated, which is higher than that of the electrode without $V(acac)_3$. Equally, the titration of Li_2O_2 in the charged electrode with $V(acac)_3$ corresponding to 0 mAh compared to the 0.2 mAh for the charged electrode without $V(acac)_3$. A possible reason is that $V(acac)_3$ promotes the decomposition of Li_2O_2 by reducing side reactions caused by highly reactive superoxide intermediate. Similar results are obtained by a modified iodometric titration method. (Table S1) These results demonstrate that the $V(acac)_3$ soluble catalyst effectively suppresses side reactions and enhances the cycle performance of the Li–O_2 cells with the reversible formation and decomposition of Li_2O_2.

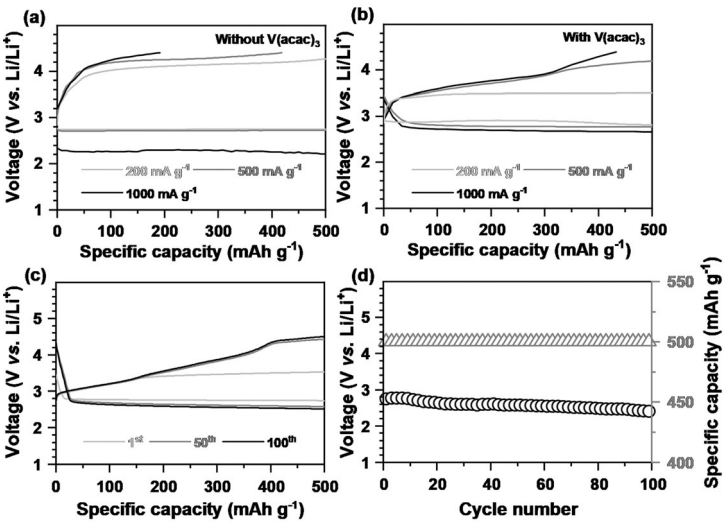

Figure 2. Discharge–charge profiles of Li–O_2 cells a) without $V(acac)_3$ and b) with $V(acac)_3$ at constant current density of 200, 500, and 1000 mA g^{-1} with a capacity limit of 500 mAh g^{-1}, c) discharge–charge profiles of Li–O_2 cells with $V(acac)_3$ at a constant current density of 200 mA g^{-1} with a capacity limit of 500 mAh g^{-1}, and d) the corresponding delivered discharge capacity and the terminal discharge voltage versus the cycle number for Li–O_2 cells with $V(acac)_3$.

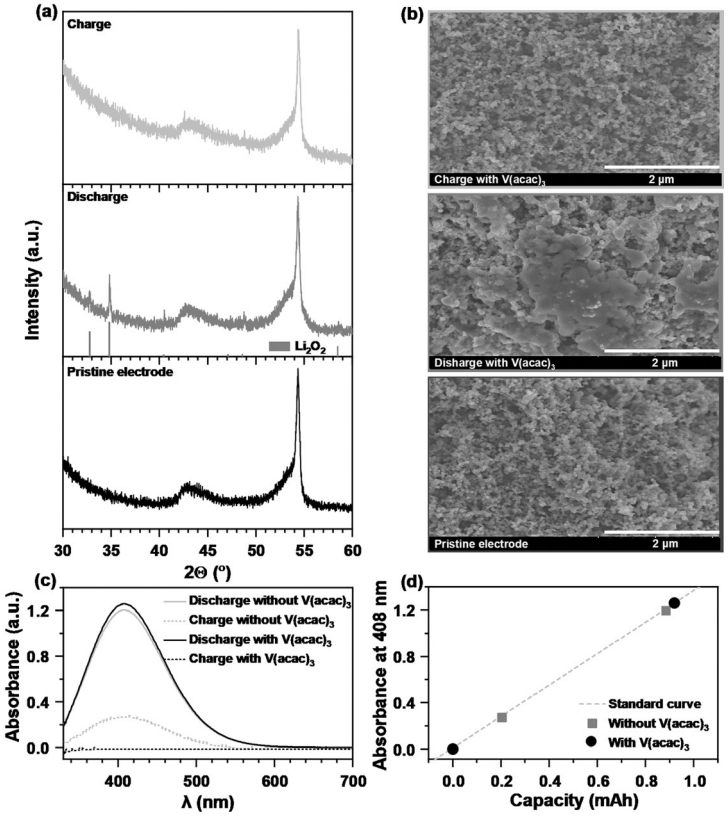

Figure 3. a) X-ray diffraction (XRD) patterns and b) scanning electron microscope (SEM) images of (from bottom to top) pristine, discharged, and recharged O_2 electrodes with the $V(acac)_3$ at a current density of 200 mA g^{-1} with a capacity limitation of 500 mAh g^{-1}, c) the UV/Vis spectra of the titanium-(IV) oxysulfate ($TiOSO_4$) solutions for O_2 electrodes at different states without and with $V(acac)_3$, and d) the corresponding capacities obtained from $TiOSO_4$-based UV/Vis spectroscopic titration. (The standard curve is obtained from Figure S7.)

To further identify the interaction of LiO_2 with the $V(acac)_3$ catalyst, density functional theory (DFT) calculations were performed. LiO_2 is found to bind to $V(acac)_3$ via the displacement of one acetylacetonate ligand (Figure S8). The binding of LiO_2 leads to a change in the magnetic moment on the V ion from 1.90 μ_B to 1.02 μ_B, indicating a change in the oxidation state from V^{III} to V^{IV}. The oxidation of V is accompanied by a charge transfer to the superoxide (O_2^-) resulting in a reduction to peroxide (O_2^{2-}), which is evident from the change in the magnetic moment on the LiO_2 moiety from $\approx$1 μ_B to $\approx$0 μ_B. The reaction of the second step is thermodynamically favorable by 0.54 eV (Figure 4a), suggesting a strong binding between LiO_2 and $V(acac)_3$ as indicated by the marked change in the absorbance from UV/Vis spectra. Based on the electrochemical measurements, in situ observations and DFT calculations, the ORR and OER mechanism of the Li–O_2 cell with $V(acac)_3$ is proposed by the Scheme in Figure 4b. During ORR, Li^+ interacts with $V(acac)_3$ to form $Li^+V(acac)_3$, which has a strong affinity with the superoxide intermediate that promotes the formation of $V(acac)_3$–LiO_2. The complex undergoes the electron transfer step in the presence of a second Li^+ to form $V(acac)_3$–Li_2O_2, which then dissociates to Li_2O_2 and $V(acac)_3$. During OER, the $V(acac)_3$ is oxidized on the surface of the electrode to form $V(acac)_3^+$, which transports electrons and facilitates the oxidation of Li_2O_2 at a lower voltage. The $V(acac)_3^+$ is then returned to its neutral form. These calculations show the bifunctional mechanism of the $V(acac)_3$ as a soluble catalyst which promotes the discharge reaction kinetics, lowers the charge voltage, decreases the side reactions, and enhances the cycle stability of the Li–O_2 cell.

In conclusion, $V(acac)_3$ has been demonstrated to be an effective bifunctional soluble catalyst for Li–O_2 batteries. $V(acac)_3$ changes the ORR reaction mechanism in Li^+-containing and Li^+-free high DN electrolytes. Especially in the electrolyte with Li^+, $V(acac)_3$ integrates with the highly active superoxide intermediate during discharge, which effectively improves the ORR kinetics and reduces side reactions in the Li–O_2 cell. Moreover, $V(acac)_3$ promotes electron transport in the electrolyte during charge, which facilitates the oxidation of Li_2O_2 at low voltage. Consequently, the Li–O_2 cells with $V(acac)_3$ exhibit a high rate performance (operating at a high current density of 1000 mA g^{-1}), low discharge and charge overpotential, and long cycle life (100 cycles at a current density of 200 mA g^{-1} with a capacity limit of 500 mAh g^{-1}). This work shows that using one soluble catalyst simultaneously addresses the instability of high DN solvents and improves cyclability in Li–O_2 batteries, which could also be applied in other metal–O_2 systems. We expect that the development of this new type of soluble catalyst will facilitate the practical use of the Li–O_2 battery with high energy density and long cycle life in the future.

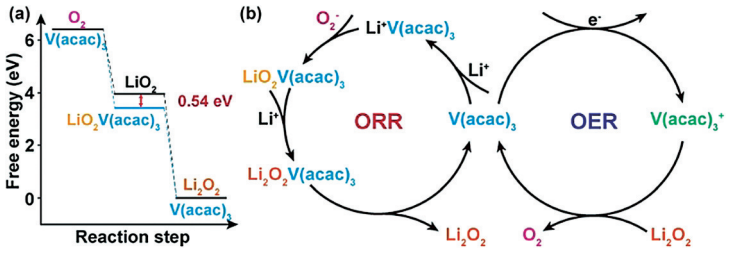

Figure 4. a) Free energy profile for the Li–O_2 cell with and without $V(acac)_3$, b) schematic illustration of ORR and OER in the cell with $V(acac)_3$.

Acknowledgements

This work was financially supported by Liaoning Revitalization Talents Program—Pan Deng Scholars (XLYC1802005), Liaoning BaiQianWan Talents Program, National Science Fund of Liaoning Province for Excellent Young Scholars, Science and Technology Innovative Talents Support Program of Shenyang (RC180166), Australian Research Council (ARC) through Discovery Early Career Researcher Award (DE150101306) and Linkage Project (LP160100927),

Faculty of Science Strategic Investment Funding 2019 of University of Newcastle, and CSIRO Energy. The computational work was supported by the Robert A. Welch Foundation Grant F-1841 and the Texas Advanced Computing Center.

Conflict of interest

The authors declare no conflict of interest.

Keywords: donor number · Li–O_2 battery · reaction mechanism · soluble catalyst · vanadium(III) acetylacetonate

How to cite: *Angew. Chem. Int. Ed.* **2019**, *58*, 12553 – 12557
Angew. Chem. **2019**, *131*, 12683 – 12687

[1] a) P. G. Bruce, S. A. Freunberger, L. J. Hardwick, J. M. Tarascon, *Nat. Mater.* **2011**, *11*, 19 – 29; b) Y. H. Zhu, Y. B. Yin, X. Yang, T. Sun, S. Wang, Y. S. Jiang, J. M. Yan, X. B. Zhang, *Angew. Chem. Int. Ed.* **2017**, *56*, 7881 – 7885; *Angew. Chem.* **2017**, *129*, 7989 – 7993; c) Y. J. Li, L. Cui, P. F. Da, K. W. Qiu, W. J. Qin, W. B. Hu, X. W. Du, K. Davey, T. Ling, S. Z. Qiao, *Adv. Mater.* **2018**, *30*, 1804653.

[2] a) D. Aurbach, B. D. McCloskey, L. F. Nazar, P. G. Bruce, *Nat. Energy* **2016**, *1*, 16128; b) X. Gao, Y. Chen, L. Johnson, P. G. Bruce, *Nat. Mater.* **2016**, *15*, 882 – 888; c) W. Zhang, Y. Shen, D. Sun, Z. Huang, Y. Huang, *Adv. Energy Mater.* **2017**, *7*, 1602938.

[3] a) P. Tan, M. Liu, Z. Shao, M. Ni, *Adv. Energy Mater.* **2017**, *7*, 1602674; b) H. Song, H. Deng, C. Li, N. Feng, P. He, H. Zhou, *Small Methods* **2017**, *1*, 1700135.

[4] Z. Lyu, Y. Zhou, W. Dai, X. Cui, M. Lai, L. Wang, F. Huo, W. Huang, Z. Hu, W. Chen, *Chem. Soc. Rev.* **2017**, *46*, 6046 – 6072.

[5] a) S. Zhang, Z. Huang, Z. Wen, L. Zhang, J. Jin, R. Shahbazian-Yassar, J. Yang, *Nano Lett.* **2017**, *17*, 3518 – 3526; b) S. M. Xu, X. Liang, Z. C. Ren, K. X. Wang, J. S. Chen, *Angew. Chem. Int. Ed.* **2018**, *57*, 6825 – 6829; *Angew. Chem.* **2018**, *130*, 6941 – 6945; c) T. Liu, Z. Liu, G. Kim, J. T. Frith, N. Garcia-Araez, C. P. Grey, *Angew. Chem. Int. Ed.* **2017**, *56*, 16057 – 16062; *Angew. Chem.* **2017**, *129*, 16273 – 16278; d) H. Zhong, J. Wang, F. Meng, X. Zhang, *Angew. Chem. Int. Ed.* **2016**, *55*, 9937 – 9941; *Angew. Chem.* **2016**, *128*, 10091 – 10095; e) T. Ling, D. Y. Yan, Y. Jiao, H. Wang, Y. Zheng, X. Zheng, J. Mao, X. W. Du, Z. Hu, M. Jaroniec, S. Z. Qiao, *Nat. Commun.* **2016**, *7*, 12876.

[6] A. C. Luntz, B. D. McCloskey, *Chem. Rev.* **2014**, *114*, 11721 – 11750.

[7] V. R. Chitturi, M. Ara, W. Fawaz, K. Y. S. Ng, L. M. R. Arava, *ACS Catal.* **2016**, *6*, 7088 – 7097.

[8] B. D. McCloskey, R. Scheffler, A. Speidel, D. S. Bethune, R. M. Shelby, A. C. Luntz, *J. Am. Chem. Soc.* **2011**, *133*, 18038 – 18041.

[9] a) Y. H. Chen, S. A. Freunberger, Z. Q. Peng, O. Fontaine, P. G. Bruce, *Nat. Chem.* **2013**, *5*, 489 – 494; b) Z. Liang, Y. C. Lu, *J. Am. Chem. Soc.* **2016**, *138*, 7574 – 7583.

[10] a) H.-D. Lim, B. Lee, Y. Zheng, J. Hong, J. Kim, H. Gwon, Y. Ko, M. Lee, K. Cho, K. Kang, *Nat. Energy* **2016**, *1*, 16066; b) J. B. Park, S. H. Lee, H. G. Jung, D. Aurbach, Y. K. Sun, *Adv. Mater.* **2018**, *30*, 1704162.

[11] H. D. Lim, H. Song, J. Kim, H. Gwon, Y. Bae, K. Y. Park, J. Hong, H. Kim, T. Kim, Y. H. Kim, X. Lepro, R. Ovalle-Robles, R. H. Baughman, K. Kang, *Angew. Chem. Int. Ed.* **2014**, *53*, 3926 – 3931; *Angew. Chem.* **2014**, *126*, 4007 – 4012.

[12] W.-J. Kwak, D. Hirshberg, D. Sharon, M. Afri, A. A. Frimer, H.-G. Jung, D. Aurbach, Y.-K. Sun, *Energy Environ. Sci.* **2016**, *9*, 2334 – 2345.

[13] B. J. Bergner, A. Schurmann, K. Peppler, A. Garsuch, J. Janek, *J. Am. Chem. Soc.* **2014**, *136*, 15054 – 15064.

[14] D. Sun, Y. Shen, W. Zhang, L. Yu, Z. Yi, W. Yin, D. Wang, Y. Huang, J. Wang, D. Wang, J. B. Goodenough, *J. Am. Chem. Soc.* **2014**, *136*, 8941 – 8946.

[15] Z. Guo, C. Li, J. Liu, Y. Wang, Y. Xia, *Angew. Chem. Int. Ed.* **2017**, *56*, 7505 – 7509; *Angew. Chem.* **2017**, *129*, 7613 – 7617.

[16] Q. Liu, A. E. S. Sleightholme, A. A. Shinkle, Y. Li, L. T. Thompson, *Electrochem. Commun.* **2009**, *11*, 2312 – 2315.

[17] C. O. Laoire, S. Mukerjee, K. Abraham, E. J. Plichta, M. A. Hendrickson, *J. Phys. Chem. C* **2009**, *113*, 20127 – 20134.

[18] R. G. Pearson, *J. Am. Chem. Soc.* **1963**, *85*, 3533 – 3539.

[19] C. O. Laoire, S. Mukerjee, K. Abraham, E. J. Plichta, M. A. Hendrickson, *J. Phys. Chem. C* **2010**, *114*, 9178 – 9186.

[20] a) L. Yang, J. T. Frith, N. Garcia-Araez, J. R. Owen, *Chem. Commun.* **2015**, *51*, 1705 – 1708; b) D. M. Itkis, D. A. Semenenko, E. Y. Kataev, A. I. Belova, V. S. Neudachina, A. P. Sirotina, M. Havecker, D. Teschner, A. Knop-Gericke, P. Dudin, A. Barinov, E. A. Goodilin, Y. Shao-Horn, L. V. Yashina, *Nano Lett.* **2013**, *13*, 4697 – 4701.

[21] Y. L. Zhang, Q. H. Cui, X. M. Zhang, W. C. McKee, Y. Xu, S. G. Ling, H. Li, G. M. Zhong, Y. Yang, Z. Q. Peng, *Angew. Chem. Int. Ed.* **2016**, *55*, 10717 – 10721; *Angew. Chem.* **2016**, *128*, 10875 – 10879.

[22] P. Singh, R. Sahai, *Aust. J. Chem.* **1969**, *22*, 1169 – 1175.

[23] H.-H. Wang, Y. J. Lee, R. S. Assary, C. Zhang, X. Luo, P. C. Redfern, J. Lu, Y. J. Lee, D. H. Kim, T.-G. Kang, E. Indacochea, K. C. Lau, K. Amine, L. A. Curtiss, *J. Phys. Chem. C* **2017**, *121*, 9657 – 9661.

Manuscript received: June 16, 2019
Accepted manuscript online: July 12, 2019
Version of record online: August 1, 2019

